Thermodynamic Description of Polymorphism in Q- and N-Rich Peptide Aggregates Revealed by Atomistic Simulation

Joshua T. Berryman,[†‡] Sheena E. Radford,[†§] and Sarah A. Harris[†‡*]
[†]Astbury Centre for Structural Molecular Biology, [‡]School of Physics and Astronomy, and [§]Institute of Molecular and Cellular Biology, University of Leeds, Leeds, United Kingdom

ABSTRACT Amyloid fibrils are long, helically symmetric protein aggregates that can display substantial variation (polymorphism), including alterations in twist and structure at the β-strand and protofilament levels, even when grown under the same experimental conditions. The structural and thermodynamic origins of this behavior are not yet understood. We performed molecular-dynamics simulations to determine the thermodynamic properties of different polymorphs of the peptide GNNQQNY, modeling fibrils containing different numbers of protofilaments based on the structure of amyloid-like cross-β crystals of this peptide. We also modeled fibrils with new orientations of the side chains, as well as a de novo designed structure based on antiparallel β-strands. The simulations show that these polymorphs are approximately isoenergetic under a range of conditions. Structural analysis reveals a dynamic reorganization of electrostatics and hydrogen bonding in the main and side chains of the Gln and Asn residues that characterize this peptide sequence. Q/N-rich stretches are found in several amyloidogenic proteins and peptides, including the yeast prions Sup35-N and Ure2p, as well as in the human poly-Q disease proteins, including the ataxins and huntingtin. Based on our results, we propose that these residues imbue a unique structural plasticity to the amyloid fibrils that they comprise, rationalizing the ability of proteins enriched in these amino acids to form prion strains with heritable and different phenotypic traits.

INTRODUCTION

Many proteins and peptides self-assemble under the appropriate experimental conditions and form insoluble filamentous structures known as amyloid fibrils (1). There is currently great interest in amyloid formation not only because of its involvement in a number of human diseases, but also because the inherent ability of proteins to self-assemble into amyloid could prove useful for designing novel nanomaterials if the assembly could be sufficiently well controlled (2). Amyloid fibrils possess distinct structural and mechanical properties, and serve a number of diverse functions in biology, including melanin deposition, bacterial film formation, and endowment of novel inheritable traits, such as in the case of yeast prions (3). Structural studies have shown that all amyloid fibrils are composed of a number of protofilaments that are wound together to produce higher-order fibrillar structures (4). Within each protofilament, the proteins or small peptides are held together in long β-sheets by backbone hydrogen-bond interactions that are oriented parallel to the fibril axis. A protofilament consists of two or more of these sheets held together by side-chain–side-chain interactions. The ability of so many peptides to form amyloid fibrils is perhaps unsurprising since a significant number of the interchain bonds are formed by the amino acid backbone, which is generic to all proteins (5). However, obtaining fully atomistic information about the structure of amyloid fibrils has proved to be a challenge because of the heterogeneity inherent in fibril samples, the inability so far to crystallize all but the smallest model peptides into a cross-β array, and the need to obtain structural information over length scales spanning Å-μm to build up a complete model of the fibril architecture. Nonetheless, x-ray structures of 3D crystals of small peptides (6,7), combined with information from techniques such as solid-state NMR (8–11), cryo-electron microscopy (12,13), transmission electron microscopy (14), electron paramagnetic resonance (15), fluorescence resonance energy transfer (16), and mutational (17) and hydrogen exchange (18) experiments offer structural insights into different fibrillar forms (4).

Although all amyloid fibrils are characterized by a cross-β structure and a filamentous morphology, fibrils formed from different peptide sequences can vary substantially in length and twist. At the molecular level, diversity in amyloid structure arises from factors such as the number of β-sheets within a protofilament, the registry of these β-sheets, the organization of the comprising β-strands, and even the degree to which all or part of the protein monomer participates in the hydrogen-bonded amyloid core (4). Although many amyloid fibrils appear to be constructed from in-register parallel (P) β-strands (19–22), antiparallel (AP) structures have also been reported (9,10,23). Even the most subtle differences in the arrangement of peptides at the atomic level, when propagated additively over many monomer units, can produce very large changes in fibril morphology at a mesoscopic level (24). This may endow each fibril type with different mechanical properties and/or biological activities (25) in vivo, as demonstrated most clearly by polymorphism in prion strains (26–29). The prion strain phenomenon has been shown to involve large-scale

Submitted October 7, 2008, and accepted for publication March 11, 2009.

*Correspondence: s.a.harris@leeds.ac.uk

Editor: Ruth Nussinov.

0006-3495/09/07/0001/11 $2.00

doi: 10.1016/j.bpj.2009.03.062

conformational differences between polymorphic forms in the case of the Sup35 yeast prion (30). Perhaps most intriguing is the sensitivity of the predominant fibril morphology to growth conditions, such as the hydrophobicity of the solvent (31), the solution pH (23), the temperature (27), the salt concentration of the buffer (32), and even whether the same solution is stirred or kept quiescent during the growth phase (23).

Here we investigated polymorphism in fibrillar assemblies using as a model the peptide GNNQQNY in atomistic molecular-dynamics (MD) simulations. In particular, we explored the thermodynamic properties of different possible polymorphs of this polypeptide sequence. Although a number of simulation studies have explored the early aggregation behavior of this sequence (33–35), the possibility that different polymorphs may have different thermodynamic properties has received less attention from theoreticians (36). GNNQQNY is particularly amenable to computational studies because a crystal structure of one possible polymorph has been reported and shown, via different space groups, to be capable of adopting a different organization of higher-order packing (6,7). Moreover, a number of distinct polymorphic forms of amyloid fibrils formed from this sequence have been identified using solid-state NMR (11), although the details of their structural diversity at the atomic level remain unresolved. Significantly, recent solid-state NMR studies of SNNFGAILSS detected both P and AP β-sheet-containing polymorphs even within the same fibril sample, and high-resolution structures have been obtained for both the P and AP forms (37,38). Here we used computational methods to design and build de novo protofilaments and the consequent fibrils that contain β-strands of GNNQQNY organized in a novel AP arrangement that has not yet been detected experimentally for this sequence, as well as P β-sheets based on the x-ray structure of this peptide, which comprises originally flat P β-sheets (6), and P β-sheet polymorphs with differing packing interactions at the interface between the two stacked β-sheets. By creating fibrils containing different numbers of protofilaments from the complementary P and AP architectures and analyzing the structural and thermodynamic properties of each of the resulting systems, we were able to explore the relationship between the stability of different polymorphs and their structural organization. The results reveal how changes in local structure can give rise to dramatic alterations in fibril morphology, and the structural origins of the thermodynamic stability of these different molecular forms.

MATERIALS AND METHODS

All MD simulations used the AMBER 8 suite of programs in conjunction with the AMBER99 force field (39). Initial coordinates for the P32 systems (pairs of 16-residue P β-sheets) were obtained from the crystal structure 1YJP (6). Initial configurations for the remaining AP32 (pairs of 16-residue AP β-sheets), P128, and AP128 (four 32-residue sheets) structures were rationally designed using the NAB molecular building tool (40). The initial conformation was constructed to maximize the hydrogen-bonding interactions within each β-sheet as well as side-chain interactions at the interface between the β-sheets. Protons were added using the LEAP module within AMBER. In most cases, the N-terminus was protonated and the C-terminus deprotonated, except for a single study of P32 and AP32 in which the C-terminus was neutralized to mimic conditions of low pH (Table 1). Partial charges for the protonated C-terminal tyrosine were obtained using Gaussian98 (41) and the ANTECHAMBER module of AMBER8. Electronic structure calculations were performed at the 6-31G** level and partial charges were assigned using the RESP charge fitting procedure. Implicitly solvated simulations used the generalized Born/surface area (GB/SA) method (42) with the Tsui and Case (43) parameters, and an interaction cutoff of 25 Å. These systems were equilibrated by performing an initial energy minimization followed by restrained MD during which the system was heated to 300 K, followed by unrestrained MD, which allowed these systems to further relax under thermal motion. For the 32-peptide model systems, this relaxation period was 15 ns; however, because of computation costs, only 5 ns of relaxation was allowed for the 128-peptide models. The stability of the aggregates and convergence of the calculations were assessed by monitoring the solute energies and root mean-square deviations (RMSDs; see Figs. S1 and S2 in the Supporting Material). In calculations using explicit solvent, the aggregates were surrounded by an octahedral periodic box of TIP3P water molecules to a minimum distance of 15 Å from the solute before equilibration using a standard multistate protocol (44). The fast particle-mesh Ewald module of AMBER8 was used to calculate long-range electrostatic interactions. All bonds to hydrogen were constrained

TABLE 1 Structural characterization of the aggregates in terms of helical pitch, shape complementarities (S_c), and electrostatic complementarities (E_c) for each interface

System	P32	AP32	P32*	AP32*	P32†	AP32†	P32′‡	32″§	P128	AP128
Monomers per sheet	16	16	16	16	16	16	16	16	32	32
No. of β-sheets	2	2	2	2	2	2	2	2	4	4
Simulation time (ns)	25	25	25	25	25	25	25	25	15	15
Helical pitch (Å)	157	174	176	192	148	215	138	166	323	480
Dry interface S_c	0.70	0.78	0.70	0.81	0.75	0.77	0.76	0.79	0.69	0.76
"Wet" interface S_c	-	-	-	-	-	-	-	-	0.81	0.73
Dry interface E_c	0.78	0.38	0.63	0.57	0.57	0.48	0.80	0.75	0.86	0.57
"Wet" interface E_c	-	-	-	-	-	-	-	-	0.44	0.53

*This simulation was run using a TIP3P explicit water model.

†Monomers in this system have protonated C-termini. All other systems retained a negative charge at the C-termini and positive N-termini.

‡This simulation was run from a starting structure in which the β-sheets are staggered relative to the crystal structure (6).

§This simulation was run from a starting structure in which the side chains within the steric zipper are locked into an alternative conformation from that found in the crystal structure (6).

Note that the S_c value for the dry interface of the 3D crystal structure of GNNQQNY (6) is 0.86. For the wet interface of the crystal, it is undefined.

using the SHAKE algorithm, allowing an integration time step of 2 fs to be used during both implicitly and explicitly solvated MD calculations. All MD simulations were performed at constant temperature (300 K) and pressure (1 atm), except for an additional pair of explicitly solvated simulations of P32 and AP32, which were performed at an elevated temperature of 370 K to demonstrate the high stability of these aggregates (see Supporting Material). The calculations were run on an Opteron-Myrinet supercomputer available at the University of Leeds.

Data analysis was performed on 1000 structures selected every 10 ps from the final 10 ns of each simulation reported in Table 1. In all cases, end strands were excluded from the analysis to avoid edge effects. Hydrogen-bond occupancies and structure RMSDs were calculated using the PTRAJ module available within AMBER. Secondary structure analysis was performed using the Dictionary of Secondary Structure of Protein (DSSP (45)). Twists were measured as the angles between successive intersheet vectors in the plane perpendicular to the fibril axis vector, using NAB (46). Energies of solvated systems were calculated using the GB/SA methodology applied to successive solute structures obtained from the explicitly solvated MD. The GB/SA method allows for the inclusion of an empirical term (based on the solvent-exposed surface area of hydrophobic residues) to account for changes in solvent entropy between P and AP aggregates, and has been used extensively to calculate changes in solvation free energy for large biomolecular systems (47–50). Shape complementarities (S_c) were analyzed using the method developed by Lawrence and Colman (51), and successfully reproduced the value of 0.86 for the steric zipper of 1YJP reported by Nelson et al. (6). Electrostatic complementarity (E_c) measurements were carried out using the method developed by McCoy et al. (52) to calculate the partly solvated Spearman correlation coefficient, and electrostatic potentials were calculated using the DELPHI program (53,54). Configurational entropies were calculated by diagonalization of the mass-weighted Cartesian coordinate covariance matrix in conjunction with the Schlitter equation (55–57). Entropies were calculated using only backbone atoms to filter out stochastic contributions from side-chain fluctuations. Molecular representations for the figures were prepared using PYMOL (58).

RESULTS

Stable polymorphs of GNNQQNY can be constructed from both P and AP β-sheets

The most basic structural unit of a protofilament consists of a pair of β-sheets stacked together within a steric zipper. In the 3D crystal structure of GNNQQNY, each separate β-sheet is P and perfectly in register (6). The stacking between a pair of these β-sheets is AP in the direction perpendicular to the long axis of the protofilament; the sheets are also staggered to allow the side chains to interdigitate within the steric zipper. To investigate whether alternative polymorphic forms of the same peptide sequence could be thermodynamically stable, we constructed two different protofilament forms of GNNQQNY made up of P and AP in register β-sheets. Coordinates for the P systems (symmetry class 1 according to the classification system of Sawaya et al. (7)) were taken from the crystal structure of GNNQQNY (6), whereas the AP system (which is equivalent to class 5 in Sawaya et al.'s (7) notation, and has not been observed experimentally to date) were designed and built in silico. MD calculations using an implicit solvation model (59) were performed for aggregates equivalent to a single protofilament comprising a pair of interdigitating β-sheets, each containing 16 β-strands (P32 and AP32), and for larger aggregates containing four β-sheets of 32 peptides, each giving a total of 128 monomers (P128 and AP128). Simulations of P32 and AP32 were also run in explicit solvent to validate these results (see Materials and Methods). In addition, simulations of P32 and AP32 were performed in which the C-termini were neutralized to mimic low pH conditions. Details of the simulations performed are summarized in Table 1.

Data showing the time series of the energy, RMSDs, helical twist, secondary structure analysis, and total hydrogen bonding over each simulation are also provided in Figs. S1–S3 and S6. Throughout the simulations, all of the polymorphs retained a high degree of structural regularity, irrespective of the number of β-sheets or their molecular organization. The stable molecular structures obtained at the end of each simulation are shown in Fig. 1. The systems designed in silico maintained interfacial packing densities comparable to those of the crystal (Table 1), indicating that our methodology for building and equilibrating novel

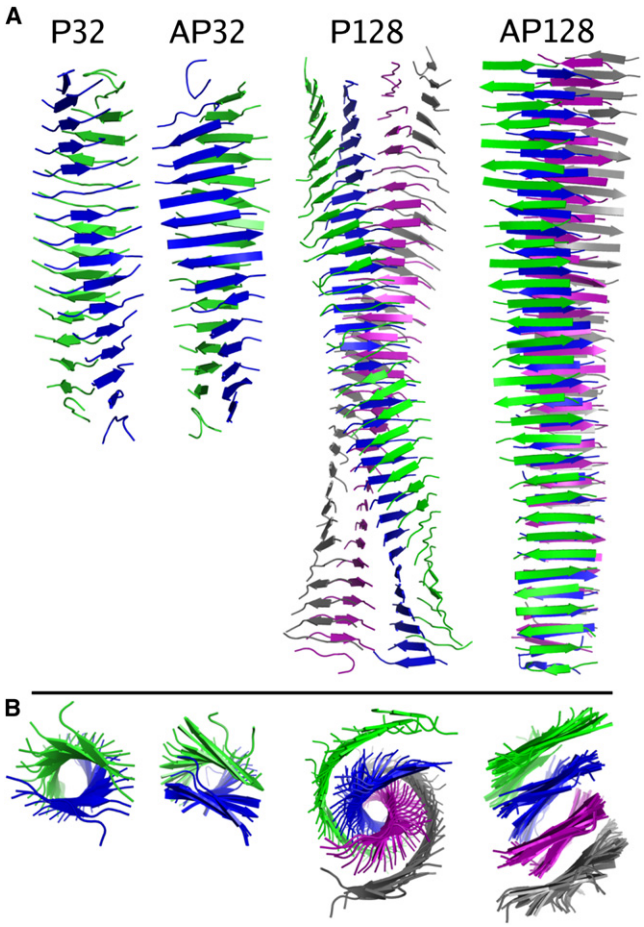

FIGURE 1 Final configurations of the MD simulations of the parallel and antiparallel β-sheet aggregates of GNNQQNY from the transverse (*A*) and axial (*B*) viewpoints. P32 and AP32 are protofilament structures containing two β-sheets each of 16 parallel (P) or antiparallel (AP) β-strands. P128 and AP128 are protofilament structures containing four β-sheets each of 32 P or AP β-strands. The structural coordinates are available in pdb format from the corresponding author on request.

polymorphs is capable of generating stable amyloid-like structures. Explicitly solvated simulations of P32 and AP32 performed at 370 K (see Figs. S4–S7) also remained stable, demonstrating that these structures remain robust even at elevated temperatures. These results illustrate that alternative molecular structures can be generated in silico for the same peptide sequence, allowing investigation of the thermodynamic rationale for polymorphism in these amyloid fibrils. Perczel et al. (60) rationalized the thermodynamic stability as amyloid using quantum chemical calculations on poly-alanine rich systems; moreover, stable MD trajectories were also recently observed for poly-glutamine aggregates at high temperatures (500 K) over timescales of 15 ns (61).

Polymorphs are closely isoenergetic but differ in morphology

The high stability of the polymorphs constructed allowed us to monitor the effects on the energetic stability of GNNQQNY aggregates due to changes in the intermolecular arrangement of monomer chains within the protofilaments. Strikingly, we found that the energetic stability of protofilaments is relatively insensitive to the molecular-level arrangement of the peptide chains, as shown in Fig. 2. The total energy per monomer is marginally in favor of the AP β-sheet when the protofilaments contain only a single pair of stacked sheets, although the two states become indistinguishable energetically when the C-termini are neutralized to mimic low pH conditions (Fig. 2). Since fibrils generally contain more than a single stacked pair of β-sheets, we also compared the energies of P and AP β-strand arrangements in protofilaments constructed from four β-sheets (P128 and AP128). The data reveal that increasing the width of the protofilaments from two to four stacked β-sheets is energetically favorable in both cases (due to the additional van der Waals

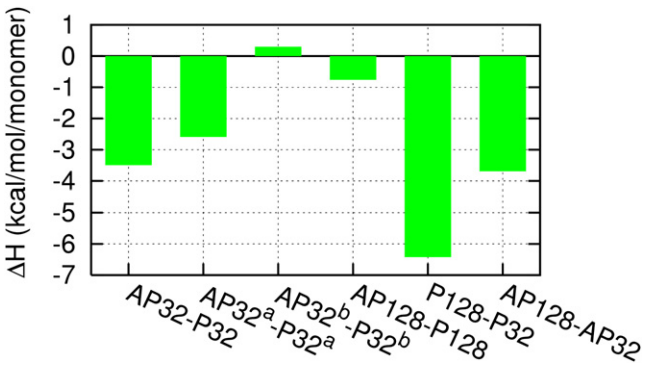

FIGURE 2 Enthalpy differences between different polymorphic forms of GNNQQNY calculated by MD simulation (note that these values contain a contribution from the solvent entropy in accordance with the GB/SA methodology). Enthalpy differences larger than 1 kcal/mol (the difference in enthalpy between equivalent simulations performed with implicit/explicit solvent) are considered significant. Simulations denoted by superscript "a" were run using explicit solvent. Monomers in systems denoted by superscript "b" had protonated C-termini. All other systems had negatively charged C-termini and positive N-termini.

interactions between buried interfaces), but alters the balance of the interfacial energies in such a way that the P and AP protofibrils have identical energy within the error of our measurements. To investigate the importance of entropic effects in determining fibril stability, we also calculated the configurational entropies of the backbone atoms of the P32 and AP32 systems from our MD trajectories (see Table S1). Although this entropic term marginally favors the P arrangement for a single pair of stacked β-sheets, again there is no significant difference in the entropy of P128 and AP128. We therefore describe the P and AP polymorphs as closely isoenergetic, since changing the number of stacked β-sheets, or the protonation state of the termini, affects the thermodynamics as significantly as changing from P to AP β-strands. We therefore expect that both polymorphs will be viable structures for this sequence, but the dominant polymorphic form will be sensitive to the growth conditions.

Alongside the thermodynamic analysis, we also characterized the structural details of each polymorph by measuring the dihedral angles of the backbone, as well as the helical pitch (Table 1 and Fig. S6). In the 3D crystal structure of GNNQQNY, the β-strands are highly pleated ($\varphi \approx -115°$; $\psi \approx 110°$) and the β-sheets are extremely flat, such that no helical period results (6). In contrast, the β-strands in P32 become more extended ($\varphi \approx -130°$; $\psi \approx 140°$) and the strands spontaneously twist within the first 100 ps of the simulation in implicit solvent, giving a left-handed sheet twist in agreement with previous studies using the GROMOS force field (62). The helical pitch of 157 Å of the parallel double β-sheet of P32 is smaller than that of AP32 (174 Å). The β-sheets also untwist as the number of stacks increases, as expected from steric considerations (63). For four stacked β-sheets, we obtain a helical pitch of 323 Å and 480 Å for P128 and AP128, respectively. This observation reconciles the relatively low values of helical pitch calculated from atomistic simulations of protofilaments by us (Table 1) and others (62) with the far larger values of 700–2000 Å that are typically measured experimentally for fibrils that contain many stacked β-sheets (13,64). Moreover, the difference in twist between P and AP protofilaments becomes more distinct as they increase in width, despite the fact that the larger aggregates are indistinguishable energetically. The data reveal, therefore, that these fibrils with different fundamental arrangements of their β-strands and different morphological features have such similar stabilities that they are closely isoenergetic, rationalizing the possibility for heterogeneity of fibril assembly unless the growth conditions are carefully manipulated such that a single fibril morphology is generated by kinetic control (26,28).

Polymorphs are closely isoenergetic because of compensating molecular interactions

The all-atom structures generated by the MD simulations of the different polymorphs of GNNQQNY provide a unique

opportunity to determine how the P and AP arrangements of β-strands within the same (nonpalindromic) sequence can give rise to fibril architectures that are approximately isoenergetic. To achieve this, a detailed analysis of the hydrogen-bonding and electrostatic interactions within the ensembles of structures that define the last 10 ns of the MD simulations of P32 and AP32 was performed. Fig. 3 compares main-chain and side-chain hydrogen-bonding interactions measured during MD for P32 and AP32. Although the majority of the hydrogen-bonding interactions evident within the crystal structure of GNNQQNY persist during the MD simulation of P32, these bonds must compete with the potential for hydrogen bonding to side chains that become accessible through thermal fluctuations. A greater number of backbone hydrogen bonds are satisfied in AP32 compared with its parallel counterpart, but fewer side-chain hydrogen bonds are occupied. One crucial difference between P32 and AP32, therefore, is that a relative loss of backbone hydrogen bonding in the former is compensated for by an increase in side-chain hydrogen bonding, resulting in total hydrogen-bond occupancies that do not differ significantly between the two polymorphs (Figs. 3 and S3). The ability of GNNQQNY to compensate in this way is a unique property of the Gln and Asn residues, since only these two amino acid side chains can both accept and donate hydrogen bonds in an analogous manner to the peptide backbone, with the distance between acceptor and donor groups on the side chains being identical to that between those on the backbone.

A comparison of the electrostatic interactions between stacked P32 and AP32 also reveals a subtle adjustment of the molecular contacts within the various polymorphic forms that allows for their energetic compensation. For zwitterionic peptides to adopt P β-stranded sheets, the axial electrostatic repulsion between like partial charges within a single β-sheet must be balanced by other favorable interactions elsewhere

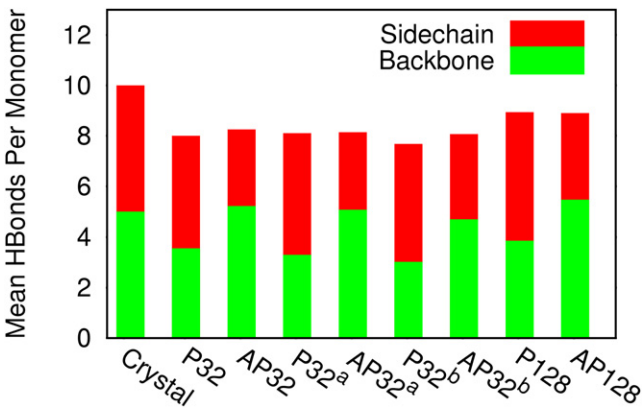

FIGURE 3 Average numbers of hydrogen bonds occupied per monomer. Occupancy was counted using an angle cutoff of 150° and a distance cutoff of 3.5Å. Simulations denoted by superscript "a" were run using explicit solvent. Monomers in systems denoted by superscript "b" had protonated C-termini. All other systems had negatively charged C-termini and positive N-termini.

within the protofilament structure. Most significantly, each of the P β-sheets in the crystal structure of GNNQQNY is packed antiparallel to another sheet within the steric zipper, bringing the charged termini into close proximity with a source of opposing charge (6). To assess the importance of side-chain interactions across the buried interfaces of the protofilament structures of P32 and AP32, electrostatic complementarities (E_c) (52) and S_c (51) were calculated for all fibril types (Table 1; the shapes and electrostatic potentials of the interior surfaces of P32 and AP32 are illustrated in Fig. 4). In both P32 and AP32, the side chains packed within the buried interfaces are orientated in such a way that they are able to form complementary electrostatic interactions with oppositely charged residues on the opposing β-strand within the steric zipper, although the manner by which this is achieved differs fundamentally. The relatively smooth internal surface of each P β-sheet in P32 contains vertical stripes of positive and negative electrostatic potential that are packed in a highly specific manner against the corresponding opposite potentials on the opposing β-strand of the steric zipper ($E_c = 0.78$). By contrast, the interior surface of the AP32 aggregate is significantly more rugged. It also has irregular patches of partial positive and negative electrostatic potential that give a weaker electrostatic interaction ($E_c = 0.38$), although the E_c values measured for both systems are comparable to those obtained for complementary protein-protein interfaces in other systems (52). The S_c measurements show that the weaker electrostatic interactions in AP32 are compensated for by tighter steric packing relative to P32 ($S_c = 0.78$ for AP32, and $S_c = 0.70$ for P32). Gln and Asn side chains possess both positive and negative partial charges and are highly flexible, with each having a side-chain conformation defined by multiple χ angles. Our calculations show that the inherent polarizablility of these residues, combined with their flexibility, allows them to adjust to maximize both favorable van der Waals and electrostatic interactions, resulting in fundamentally different polymorphic forms with similar thermodynamic stabilities.

Polymorphism can arise from variation within the steric zipper

To determine whether variation in the steric packing between stacked β-sheets can also generate polymorphs with distinct morphologies, we also performed MD simulations of aggregates of GNNQQNY designed with different interactions between the pair of stacked β-sheets, as shown in Fig. 5. In the first of these simulations (P32′), the two β-sheets were staggered relative to each other to decrease the size of the interface associated with the steric zipper. In the second simulation (P32″), alternative rotamer angles were selected for the asparagine side-chains of residues 2 and 6 in such a way as to lock the interdigitated side chains into a subtly different conformation. Fig. 5 compares the steric zippers in the starting structures (Fig. 5 *A*) and the energy-minimized,

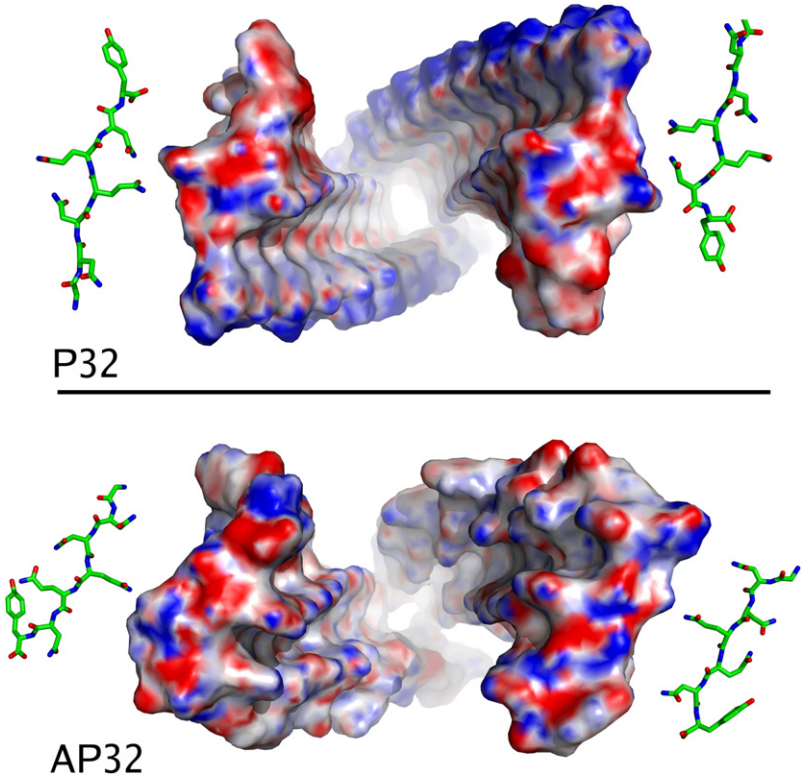

FIGURE 4 Electrostatic potentials at the inner surfaces of the steric zippers for P32 and AP32 are shown displaced relative to each other for clarity. Red and blue indicate negative and positive potentials, respectively (color available online only). Stick structures show the conformations of the topmost peptide in each sheet.

time-averaged structures (Fig. 5 *B*) for the central four strands of P32, AP32, P32′, and P32″.

Although all structures remained stable, the reduced interactions within the steric zipper in P32′ (the interfacial area in the staggered P32′ structure is reduced to 99 Å^2/monomer compared with 131 Å^2/monomer for P32) produced aggregates with a lower β-sheet content, reduced hydrogen-bonding interactions (P32′ has 6.5 hydrogen bonds per monomer compared with 8.0 per monomer for P32), and increased structural disorder, as shown in Fig. 6 (*left*). Moreover, this change in conformation incurred an enthalpic penalty of 3.2 kcal/mol/monomer relative to P32, which is similar in magnitude to the difference in enthalpies between P32 and AP32. Although the starting conformation for P32″ was generated by a minor perturbation of the crystal structure, a complex equilibration procedure was required to

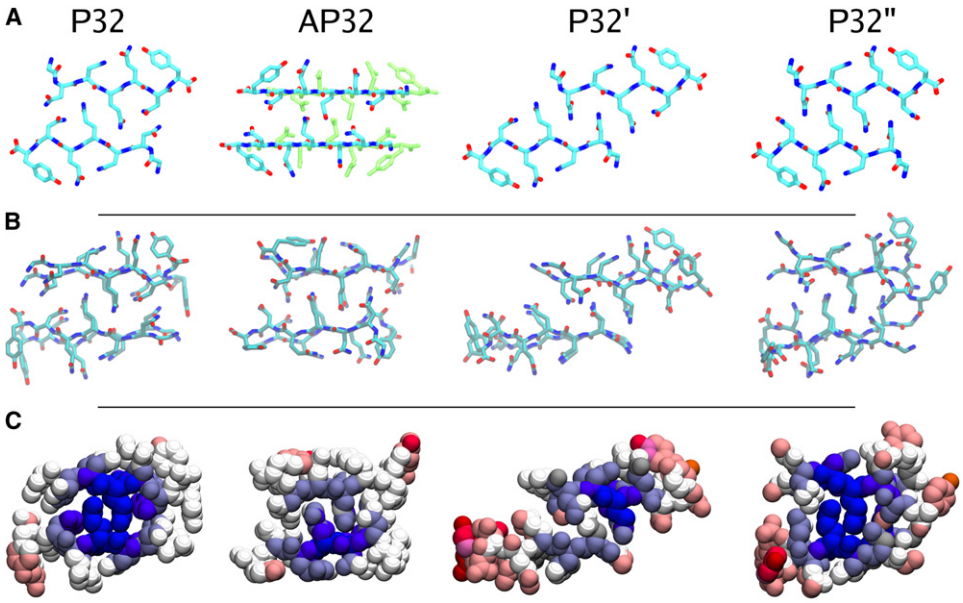

FIGURE 5 Structures of the central four-monomer sections of the P32, AP32, P32′, and P32″ models. (*A*) The steric zippers of the initial structures. (*B*) Energy-minimized average structures of the steric zippers taken over the 10 ns data production run. (*C*) The heavy atoms are colored by the RMSD from the average structure, with blue indicating the least mobile atoms (minimum RMSD = 0.25Å) and red indicating the most mobile (maximum RMSD = 6.13Å) (color available online only).

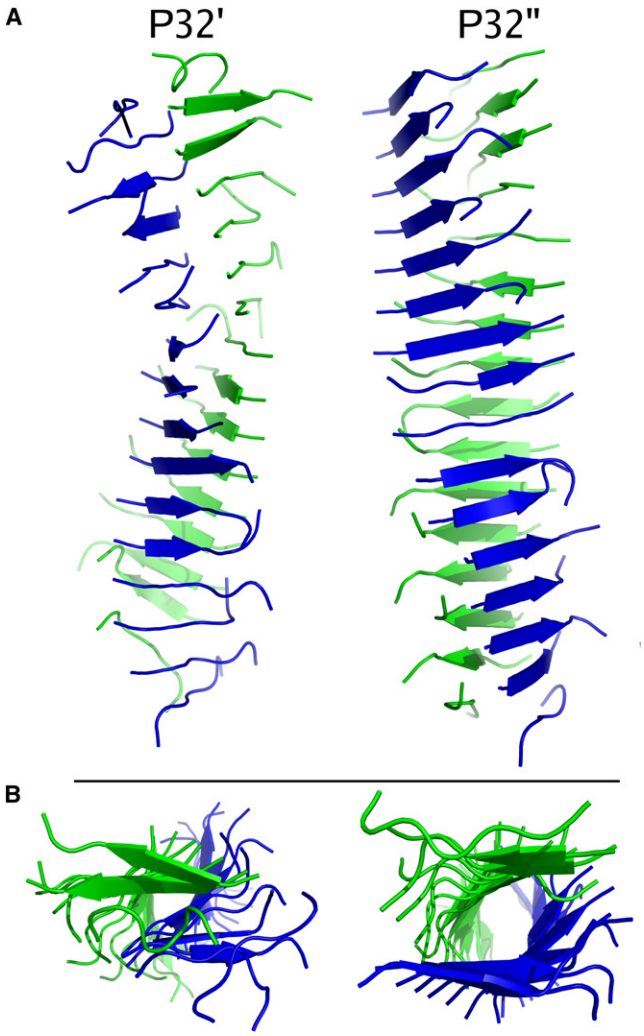

FIGURE 6 Final structures of the P32′ and P32″ systems after a 10 ns data production run in (*A*) transverse and (*B*) axial views.

generate stable aggregates for this system. The initial simulations produced aggregates containing a mixture of ordered β-sheets separated by disordered regions. We then adopted an iterative procedure in which new starting structures for MD were produced by duplicating the sections with the highest β-sheet content (thereby generating aggregates of the required size); this process was continued until the structures remained stable when subjected to MD. The final structure obtained for P32″ after a 10 ns production run is shown in Fig. 6 (*right*). This novel conformation is characterized by increased disorder at the C-termini of the peptide strands, reducing the number of hydrogen bonds per monomer from 8.0 in P32 to 7.6 in P32″. This is due to conformational crowding within the steric zipper, which extends the C-termini away from the N-termini of the opposing sheets. In contrast to P32′, the P32″ polymorph is very closely isoenergetic with P32 (the average enthalpy was 1.2 kcal/mol/monomer lower than P32) because this loss of hydrogen bonding is compensated for by increased interfacial interaction and higher S_c between the β-sheets (Table 1). The P32′ and P32″ polymorphs have helical pitches of 138 Å and 166 Å, respectively (Table 1). Therefore, as observed for P32 and AP32, we observe a reduction in helical twist with increased intersheet interaction within these polymorphs, in agreement with mesoscopic models of peptide aggregation (65). These simulations show that polymorphs generated from subtle rearrangements of side chains, as well as from fundamental changes in β-sheet structure (e.g., switching from P to AP β-sheets) can give rise to distinct morphologies while maintaining similar energetic stabilities.

DISCUSSION

Polymorphism is favored by the unique properties of Asn and Gln residues

Gln- and Asn-rich sequences are found in a variety of eukaryotic proteins and may have been positively selected during evolution (66), suggesting that sequences enriched in these residues may provide a selective advantage to the organism in which they are contained. In addition to their roles in transcriptional activation, histone deacetylation, and nuclear pore sieving (67–69), proteins that contain regions rich in Gln and Asn residues are renowned for their tendency to assemble into amyloid fibrils, resulting in devastating neurological disorders (70). Thus, evolution has had to balance the benefits and threats of these low-complexity sequences. The most striking characteristic of the aggregates associated with Q/N-rich sequences in yeasts is their ability to form many different structures (strains) depending on the precise sequence, growth conditions, or physical environment, and to pass these strains on to new generations, endowing inheritable phenotypic traits (71). Although it is widely accepted that amyloid fibrils possess a common cross-β architecture, possibly based on a generic β-spine (4), the extent and nature of structural diversity in amyloid fibrils, particularly those formed from the same sequence, remain to be resolved.

In this work we performed structural and thermodynamic analyses of fibrillar polymorphs of GNNQQNY peptides, building on crystallographic information about the structure of this sequence in 3D arrays (6). By constructing putative amyloid fibrils from this sequence involving two fundamentally different structures containing P and AP β-sheets (the latter a polymorph that has not yet been found for this sequence experimentally (7)), we were able to show that protofilaments made from these different molecular arrangements of β-strands are approximately isoenergetic, despite changes in the pattern and balance of backbone/side-chain hydrogen bonding and alternative stacking of partial charges in the different interfaces formed within the steric zipper. Moreover, we show that subtle changes in side-chain packing within a steric zipper without alterations in β-strand orientation can also produce protofilaments with different

morphologies. Most importantly, as well as possessing different surface properties, these polymorphs also result in distinct properties at the mesoscale, as revealed by variations in their helical pitch. Consequently, each polymorph might be expected to possess very different physical and biological properties, reminiscent of the properties of different prion strains (27,72). The range of surface electrostatic properties is likely to have particular relevance for the aggregation behavior with respect to changes of solvent (73), and differences in the strength of backbone hydrogen bonding should lead to very different dynamic and therefore kinetic properties of the different fibrillar forms (74).

Implications for non-Q/N-containing sequences

Based on the results presented here, we propose that Gln- and Asn-rich sequences should be especially prone to forming multiple amyloid structures (strains), since these amino acids are able to form a uniquely diverse range of molecular interactions. First, their side chains are able to donate and accept hydrogen bonds in an manner analogous to that of the peptide backbone itself, providing opportunities for both main-chain–side-chain and side-chain–side-chain hydrogen bonding. As a consequence, the hydrogen-bonding capacity of these sequences can be readily satisfied irrespective of the arrangement of the β-strands (P or AP), their register (and hence the number of main-chain–main-chain hydrogen bonds), or the organization and arrangement of protofilament stacking. Such structural plasticity also rationalizes the ability of these sequences to form different structures as growth conditions (e.g., temperature, pH, and ionic strength) are altered (75). Second, since their side chains are polar and flexible, Gln and Asn residues are inherently polarizable and can adjust to accommodate different electrostatic environments, as demonstrated by the fundamentally different, yet still complementary, arrangement of electrostatic interactions in P32 and AP32. Such behavior is also seen in the array of interactions formed by these residues in soluble proteins (76). By contrast with amyloid fibrils formed from more complex sequences, therefore, those formed from Q/N-rich sequences may be able to access the full arsenal of amyloid architectures (7) since optimal packing may be achieved regardless of the organization of the underlying secondary structural elements. Such properties rationalize the ability to maintain prion strains in Q/N-rich sequences in which the amino acids have been shuffled (77,78), and supports the view that the ability to switch on new functions by capitalizing on structural plasticity in prion-like fibrils may prove to be a selective advantage for organisms in which growth conditions may change. The extent to which energetic compensation (which is necessary for the formation of polymorphs and strains) is specific to Q/N-rich sequences is currently unclear and further work involving both experiment and simulation will be needed to reveal the true extent of structural diversity in Q/N-rich amyloid strains, as well as in amyloid fibrils formed from more complex sequences. In the case of Q/N-rich sequences, introducing amino acids with a reduced ability to form a multitude of interactions, including those with more stringent stereochemical constraints on packing, would be expected to reduce the possibility of strains by stabilizing one (or a few) structures relative to others, as has been found in other examples of protein folding and assembly reactions (79,80). Further systematic studies using MD may thus provide a route to determine the relationship between sequence complexity and polymorphism, and could also provide a useful route toward understanding the structural and energetic characteristics of species that are able to nucleate assemblies that presumably contain only a small number of β-strands (33,35,81). Furthermore, the approach taken may also aid in the quest to design and produce highly organized and well-defined amyloid architectures for structural and functional analyses, as well as for nanotechnological use.

Importance of kinetic trapping and nucleation in polymorphism

In this study we investigated the different thermodynamic stabilities of a number of polymorphic forms of GNNQQNY. Although polymorphs constructed from P/AP β-sheets can have similar energies, conversion between different fibrillar forms is prevented by an extremely large kinetic barrier, ensuring that the fidelity of fibril ''reproduction'' is maintained. Once the protofilaments have formed, switching to an alternative state would require dissolution into the monomeric form and subsequent fibril regrowth. Experiments on the $A\beta_{(1-40)}$ peptide have shown that fibril morphology is self-propagating when amyloid is grown from preformed seeds (26), illustrating the importance of kinetic trapping in amyloid growth. Very often, a single fibril morphology will be strongly predominant under specific growth conditions, even when the smallest perturbation (such as stirring) is sufficient to produce an alternative (and possibly isoenergetic) fibrillar form. This extreme selectivity is a characteristic of nucleated processes, wherein the dominant morphology grows from the polymorph with the lowest nucleation barrier. This polymorph will then be kinetically trapped, and will persist even if the resultant fully grown fibers are not in the most favorable thermodynamic state. Consequently, the polymorphic form obtained may well be kinetically rather than thermodynamically controlled. However, the relative importance of thermodynamic and kinetic factors in amyloid growth remains unknown, and is likely to be highly system-specific. Nucleated processes are extremely selective because very small perturbations of the free energy close to the top of the free-energy barrier imply extremely large changes in the nucleation and growth rates due to the exponential nature of the Boltzmann factor. Our calculations on amyloid-like aggregates show that because of the compensatory nature of the

interactions between Gln and Asn residues, the difference in energy between polymorphs is small enough to ensure that even minor changes in the experimental conditions (such as decreasing the pH or using agitation) will be sufficient to switch the thermodynamic balance between different conformational states. It is perhaps not surprising, therefore, to find selection for Q/N-rich sequences in organisms that have to adapt readily to change, since such sequences seem ideally placed to form an array of fibril architectures that are stable, can endow unique structural and functional properties, and form by a mechanism that is exquisitely balanced to allow rapid adaptation after changes in sequence or in growth conditions.

SUPPORTING MATERIAL

One table and seven figures are available at http://www.biophysj.org/biophysj/supplemental/S0006-3495(09)00853-4.

We thank Geoff Wells for providing partial charges for the protonated monomers, and Charlie Laughton for providing the code to calculate the configuration entropy.

J.T.B. received a Doctoral Training Centre studentship from the Engineering and Physical Sciences Research Council.

REFERENCES

1. Jahn, T. R., and S. E. Radford. 2008. Folding versus aggregation: polypeptide conformations on competing pathways. *Arch. Biochem. Biophys.* 469:100–117.
2. Smith, J. F., T. P. J. Knowles, C. M. Dobson, C. E. MacPhee, and M. E. Welland. 2006. Characterization of the nanoscale properties of individual amyloid fibrils. *Proc. Natl. Acad. Sci. USA.* 103:15806–15811.
3. Chiti, F., and C. M. Dobson. 2006. Protein misfolding, functional amyloid, and human disease. *Annu. Rev. Biochem.* 75:333–366.
4. Nelson, R., and D. Eisenberg. 2006. Structural models of amyloid-like fibrils. *Adv. Protein Chem.* 73:235–282.
5. Fandrich, M., and C. M. Dobson. 2002. The behaviour of polyamino acids reveals an inverse side chain effect in amyloid structure formation. *EMBO J.* 21:5682–5690.
6. Nelson, R., M. R. Sawaya, M. Balbirnie, A. A. Madsen, C. Riekel, et al. 2005. Structure of the cross-β spine of amyloid-like fibrils. *Nature.* 435:773–778.
7. Sawaya, M. R., S. Sambashivan, R. Nelson, M. I. Ivanova, S. A. Sievers, et al. 2007. Atomic structures of amyloid cross-β spines reveal varied steric zippers. *Nature.* 447:453–457.
8. Jaroniec, C. P., C. E. MacPhee, V. S. Bajaj, M. T. McMahon, C. M. Dobson, et al. 2004. High-resolution molecular structure of a peptide in an amyloid fibril determined by magic angle spinning NMR spectroscopy. *Proc. Natl. Acad. Sci. USA.* 101:711–716.
9. Gordon, D. J., J. J. Balbach, R. Tycko, and S. C. Meredith. 2004. Increasing the amphiphilicity of an amyloidogenic peptide changes the β-sheet structure in the fibrils from antiparallel to parallel. *Biophys. J.* 86:428–434.
10. Bu, Z., Y. Shi, D. J. E. Callaway, and R. Tycko. 2007. Molecular alignment within β-sheets in Aβ 14–23 fibrils: solid-state NMR experiments and theoretical predictions. *Biophys. J.* 92:594–602.
11. van der Wel, P. C. A., J. R. Lewandowski, and R. G. Griffin. 2007. Solid-state NMR study of amyloid nanocrystals and fibrils formed by the peptide GNNQQNY from yeast prion protein Sup35p. *J. Am. Chem. Soc.* 129:5117–5130.
12. Sachse, C., C. Xu, K. Wieligmann, S. Diekmann, N. Grigorieff, et al. 2006. Quaternary structure of a mature amyloid fibril from Alzheimer's Aβ (1–40) peptide. *J. Mol. Biol.* 362:347–354.
13. Jimenez, J. L., E. J. Nettleton, M. Bouchard, C. V. Robinson, C. M. Dobson, et al. 2002. The protofilament structure of insulin amyloid fibrils. *Proc. Natl. Acad. Sci. USA.* 99:9196–9201.
14. Vitrenko, Y. A., E. O. Gracheva, J. E. Richmond, and S. W. Liebman. 2007. Visualization of aggregation of the Rnq1 prion domain and cross-seeding interactions with Sup35NM. *J. Biol. Chem.* 282:1779–1787.
15. Cobb, N. J., F. D. Sonnichsen, H. McHaourab, and W. K. Surewicz. 2007. Molecular architecture of human prion protein amyloid: a parallel, in-register β-structure. *Proc. Natl. Acad. Sci. USA.* 104:18946–18951.
16. Deng, W., A. Cao, and L. Lai. 2008. Distinguishing the cross-β spine arrangements in amyloid fibrils using FRET analysis. *Protein Sci.* 17:1102–1105.
17. Koo, B. W., J. A. Hebda, and A. D. Miranker. 2008. Amide inequivalence in the fibrillar assembly of islet amyloid polypeptide. *Protein Eng. Des. Sel.* 21:147–154.
18. Kardos, J., D. Okuno, T. Kawai, Y. Hagihara, N. Yumoto, et al. 2005. Structural studies reveal that the diverse morphology of β (2)-microglobulin aggregates is a reflection of different molecular architectures. *Biochim. Biophys. Acta.* 1753:108–120.
19. Petkova, A. T., W. M. Yau, and R. Tycko. 2006. Experimental constraints on quaternary structure in Alzheimer's β-amyloid fibrils. *Biochemistry.* 45:498–512.
20. Shewmaker, F., R. B. Wickner, and R. Tycko. 2006. Amyloid of the prion domain of Sup35p has an in-register parallel β-sheet structure. *Proc. Natl. Acad. Sci. USA.* 103:19574–19579.
21. Chen, M., M. Margittai, J. Chen, and R. Langen. 2007. Investigation of α-synuclein fibril structure by site-directed spin labeling. *J. Biol. Chem.* 282:24970–24979.
22. Kajava, A. V., U. Baxa, R. B. Wickner, and A. C. Steven. 2004. A model for Ure2p prion filaments and other amyloids: the parallel superpleated β-structure. *Proc. Natl. Acad. Sci. USA.* 101:7885–7890.
23. Petkova, A. T., G. Buntkowsky, F. Dyda, R. D. Leapman, W.-M. Yau, et al. 2004. Solid state NMR reveals a pH-dependent antiparallel β-sheet registry in fibrils formed by a β-amyloid peptide. *J. Mol. Biol.* 335:247–260.
24. Makabe, K., D. McElheny, V. Tereshko, A. Hilyard, G. Gawlak, et al. 2006. Atomic structures of peptide self-assembly mimics. *Proc. Natl. Acad. Sci. USA.* 103:17753–17758.
25. Alexandrov, I. M., A. B. Vishnevskaya, M. D. Ter-Avanesyan, and V. V. Kushnirov. 2008. Appearance and propagation of polyglutamine-based amyloids in yeast: tyrosine residues enable polymer fragmentation. *J. Biol. Chem.* 283:15185–15192.
26. Petkova, A. T., R. D. Leapman, Z. Guo, W.-M. Yau, M. P. Mattson, et al. 2005. Self-propagating, molecular-level polymorphism in Alzheimer's β-amyloid fibrils. *Science.* 307:262–265.
27. Tanaka, M., S. R. Collins, B. H. Toyama, and J. S. Weissman. 2006. The physical basis of how prion conformations determine strain phenotypes. *Nature.* 442:585–589.
28. Kodali, R., and R. Wetzel. 2007. Polymorphism in the intermediates and products of amyloid assembly. *Curr. Opin. Struct. Biol.* 17:48–57.
29. Pedersen, J. S., and D. E. Otzen. 2008. Amyloid a state in many guises: survival of the fittest fibril fold. *Protein Sci.* 17:2–10.
30. Toyama, B. H., M. J. S. Kelly, J. D. Gross, and J. S. Weissman. 2007. The structural basis of yeast prion strain variants. *Nature.* 449:233–237.
31. Yamaguchi, K., H. Naiki, and Y. Goto. 2006. Mechanism by which the amyloid-like fibrils of a β2-microglobulin fragment are induced by fluorine-substituted alcohols. *J. Mol. Biol.* 363:279–288.
32. Gosal, W. S., I. J. Morten, E. W. Hewitt, D. A. Smith, N. H. Thomson, et al. 2005. Competing pathways determine fibril morphology in the self-assembly of β2-microglobulin into amyloid. *J. Mol. Biol.* 351: 850–864.

33. Meli, M., G. Morra, and G. Colombo. 2008. Investigating the mechanism of peptide aggregation: insights from mixed Monte Carlo-molecular dynamics simulations. *Biophys. J.* 94:4414–4426.
34. Zhang, Z., H. Chen, H. Bai, and L. Lai. 2007. Molecular dynamics simulations on the oligomer-formation process of the GNNQQNY peptide from yeast prion protein Sup35. *Biophys. J.* 93:1484–1492.
35. Zheng, J., B. Ma, C.-J. Tsai, and R. Nussinov. 2006. Structural stability and dynamics of an amyloid-forming peptide GNNQQNY from the yeast prion Sup-35. *Biophys. J.* 91:824–833.
36. Ma, B., and R. Nussinov. 2006. Simulations as analytical tools to understand protein aggregation and predict amyloid conformation. *Curr. Opin. Chem. Biol.* 10:445–452.
37. Madine, J., E. Jack, P. G. Stockley, S. E. Radford, L. C. Serpell, et al. 2008. Structural insights into the polymorphism of amyloid-like fibrils formed by region 20–29 of amylin revealed by solid-state NMR and X-ray fiber diffraction. *J. Am. Chem. Soc.* 130:14990–15001.
38. Nielsen, J. T., M. Bjerring, M. D. Jeppesen, R. O. Pedersen, J. M. Pedersen, et al. 2009. Unique identification of supramolecular structures in amyloid fibrils by solid-state NMR spectroscopy. *Angew. Chem. Int. Ed. Engl.* 48:2118–2121.
39. Case, D. A., T. A. Darden, T. E. Cheatham, C. L. Simmerling, J. Wang, et al. 2004. AMBER8. University of California, San Francisco, CA.
40. Macke, T., and D. A. Case. 1998. Modeling unusual nucleic acid structures. *In* Molecular Modeling of Nucleic Acids. N. B. Leontes and J. SantaLucia, editors. American Chemical Society, Washington, DC. 379–393.
41. Frisch, D. M. J., G. W. Trucks, H. B. Schlegel, G. E. Scuseria, M. A. Robb, et al. 1998. Gaussian 98. Gaussian Inc, Pittsburgh, PA.
42. Hawkins, G. D., C. J. Cramer, and D. G. Truhlar. 1996. Parametrized models of aqueous free energies of solvation based on pairwise descreening of solute atomic charges from a dielectric medium. *J. Phys. Chem.* 100:19824–19839.
43. Tsui, V., and D. A. Case. 2000. Theory and applications of the generalized Born solvation model in macromolecular simulations. *Biopolymers.* 56:275–291.
44. Shields, G. C., C. A. Laughton, and M. Orozco. 1997. Molecular dynamics simulations of the d(T·A·T) triple helix. *J. Am. Chem. Soc.* 119:7463–7469.
45. Kabsch, W., and C. Sander. 1983. Dictionary of protein secondary structure: pattern recognition of hydrogen-bonded and geometrical features. *Biopolymers.* 22:2577–2637.
46. Brown, R. A., and D. A. Case. 2006. Second derivatives in generalized Born theory. *J. Comput. Chem.* 27:1662–1675.
47. Harris, S. A., E. Gavathiotis, M. S. Searle, M. Orozco, and C. A. Laughton. 2001. Cooperativity in drug-DNA recognition: a molecular dynamics study. *J. Am. Chem. Soc.* 123:12658–12663.
48. Gohlke, H., C. Kiel, and D. A. Case. 2003. Insights into protein-protein binding by binding free energy calculation and free energy decomposition for the Ras-Raf and Ras-RalGDS complexes. *J. Mol. Biol.* 330:891–913.
49. Harris, S. A., Z. A. Sands, and C. A. Laughton. 2005. Molecular dynamics simulations of duplex stretching reveal the importance of entropy in determining the biomechanical properties of DNA. *Biophys. J.* 88:1684–1691.
50. Wang, H., and C. A. Laughton. 2007. Molecular modelling methods for prediction of sequence-selectivity in DNA recognition. *Methods.* 42:196–203.
51. Lawrence, M. C., and P. M. Colman. 1993. Shape complementarity at protein/protein interfaces. *J. Mol. Biol.* 234:946–950.
52. McCoy, A. J., E. V. Chandana, and P. M. Colman. 1997. Electrostatic complementarity at protein/protein interfaces. *J. Mol. Biol.* 268:570–584.
53. Gilson, M. K., and B. Honig. 1988. Calculation of the total electrostatic energy of a macromolecular system: solvation energies, binding energies, and conformational analysis. *Proteins.* 4:7–18.
54. Nicholls, A., and B. Honig. 1991. A rapid finite difference algorithm, utilizing successive over-relaxation to solve the Poisson-Boltzmann equation. *J. Comput. Chem.* 12:435–445.
55. Schlitter, J. 1993. Estimation of absolute and relative entropies of macromolecules using the covariance-matrix. *Chem. Phys. Lett.* 215: 617–621.
56. Wlodek, S. T., T. W. Clark, L. R. Scott, and J. A. McCammon. 1997. Molecular dynamics of acetylcholinesterase dimer complexed with tacrine. *J. Am. Chem. Soc.* 119:9513–9522.
57. Meyer, T., C. Ferrer-Costa, A. Perez, M. Rueda, A. Bidon-Chanal, et al. 2006. Essential dynamics: a tool for efficient trajectory compression and management. *J. Chem. Theory Comput.* 2:251–258.
58. DeLano, W. L. 2002. The PyMOL Molecular Graphics System. DeLano Scientific, Palo Alto, CA.
59. Cramer, C. J., and D. G. Truhlar. 1999. Implicit solvation models: equilibria, structure, spectra, and dynamics. *Chem. Rev.* 99:2161–2200.
60. Perczel, A., P. Hudaky, and V. K. Palfi. 2007. Dead-end street of protein folding: thermodynamic rationale of amyloid fibril formation. *J. Am. Chem. Soc.* 129:14959–14965.
61. Esposito, L., A. Paladino, C. Pedone, and L. Vitagliano. 2008. Insights into structure, stability, and toxicity of monomeric and aggregated polyglutamine models from molecular dynamics simulations. *Biophys. J.* 94:4031–4040.
62. Esposito, L., C. Pedone, and L. Vitagliano. 2006. Molecular dynamics analyses of cross-β spine steric zipper models: β-sheet twisting and aggregation. *Proc. Natl. Acad. Sci. USA.* 103:11533–11538.
63. Aggeli, A., I. A. Nyrkova, M. Bell, R. Harding, L. Carrick, et al. 2001. Hierarchical self-assembly of chiral rod-like molecules as a model for peptide β-sheet tapes, ribbons, fibrils, and fibers. *Proc. Natl. Acad. Sci. USA.* 98:11857–11862.
64. Gosal, W. S., S. L. Myers, S. E. Radford, and N. H. Thomson. 2006. Amyloid under the atomic force microscope. *Protein Pept. Lett.* 13:261–270.
65. Fishwick, C. W. G., A. J. Beevers, L. M. Carrick, C. D. Whitehouse, A. Aggeli, et al. 2003. Structures of helical β-tapes and twisted ribbons: the role of side-chain interactions on twist and bend behavior. *Nano Lett.* 3:1475–1479.
66. Michelitsch, M. D., and J. S. Weissman. 2000. A census of glutamine/asparagine-rich regions: implications for their conserved function and the prediction of novel prions. *Proc. Natl. Acad. Sci. USA.* 97:11910–11915.
67. Wilkins, R. C., and J. T. Li. 1999. DNA distortion and multimerization: novel functions of the glutamine-rich domain of GAGA factor. *J. Mol. Biol.* 285:515–525.
68. Guo, L., A. Han, D. L. Bates, J. Cao, and L. Chen. 2007. Crystal structure of a conserved N-terminal domain of histone deacetylase 4 reveals functional insights into glutamine-rich domains. *Proc. Natl. Acad. Sci. USA.* 104:4297–4302.
69. Melcak, I., A. Hoelz, and G. Blobel. 2007. Structure of Nup58/45 suggests flexible nuclear pore diameter by intermolecular sliding. *Science.* 315:1729–1732.
70. Gatchel, J. R., and H. Y. Zoghbi. 2005. Diseases of unstable repeat expansion: mechanisms and common principles. *Nat. Rev. Genet.* 6: 743–755.
71. Shorter, J., and S. Lindquist. 2005. Prions as adaptive conduits of memory and inheritance. *Nat. Rev. Genet.* 6:435–450.
72. Duennwald, M. L., S. Jagadish, P. J. Muchowski, and S. Lindquist. 2006. Flanking sequences profoundly alter polyglutamine toxicity in yeast. *Proc. Natl. Acad. Sci. USA.* 103:11045–11050.
73. Liang, Y., S. V. Pingali, A. S. Jogalekar, J. P. Snyder, P. Thiyagarajan, et al. 2008. Cross-strand pairing and amyloid assembly. *Biochemistry.* 47:10018–10026.
74. Pappu, R. V., X. Wang, A. Vitalis, and S. L. Crick. 2008. A polymer physics perspective on driving forces and mechanisms for protein aggregation. *Arch. Biochem. Biophys.* 469:132–141.

75. Chien, P., J. S. Weissman, and A. H. DePace. 2004. Emerging principles of conformation-based prion inheritance. *Annu. Rev. Biochem.* 73:617–656.

76. Singh, J., and J. M. Thornton. 1992. Atlas of Protein Side-Chain Interactions. IRL Press, Oxford, UK.

77. Ross, E. D., H. K. Edskes, M. J. Terry, and R. B. Wickner. 2005. Primary sequence independence for prion formation. *Proc. Natl. Acad. Sci. USA.* 102:12825–12830.

78. Liu, Y., H. Wei, J. Wang, J. Qu, W. Zhao, et al. 2007. Effects of randomizing the Sup35NM prion domain sequence on formation of amyloid fibrils in vitro. *Biochem. Biophys. Res. Commun.* 353:139–146.

79. Hill, R. B., D. P. Raleigh, A. Lombardi, and W. F. DeGrado. 2000. De novo design of helical bundles as models for understanding protein folding and function. *Acc. Chem. Res.* 33:745–754.

80. Wurth, C., W. Kim, and M. H. Hecht. 2006. Combinatorial approaches to probe the sequence determinants of protein aggregation and amyloidogenicity. *Protein Pept. Lett.* 13:279–286.

81. Gsponer, J., U. Haberthur, and A. Caflisch. 2003. The role of side-chain interactions in the early steps of aggregation: molecular dynamics simulations of an amyloid-forming peptide from the yeast prion Sup35. *Proc. Natl. Acad. Sci. USA.* 100:5154–5159.